Structural and Physical Properties of the Heavy Fermion Metal $Ce_2NiAl_6Si_5$

Jiawen Zhang[1], Jinyu Wu[1], Ye Chen[1], Rui Li[1], Michael Smidman[1], Yu Liu[1*], Yu Song[1*], and Huiqiu Yuan[1,2,3*]

[1]*Center for Correlated Matter and School of Physics, Zhejiang University, Hangzhou 310058, China*
[2]*State Key Laboratory of Silicon and Advanced Semiconductor Materials, Zhejiang University, Hangzhou 310058, China*
[3]*Collaborative Innovation Center of Advanced Microstructures, Nanjing 210093, China*

(Received 27 November 2024; accepted manuscript online 11 December 2024)

Strongly correlated electrons at the verge of quantum criticality give rise to unconventional phases of matter and behaviors, with the discovery of new quantum-critical materials driving synergistic experimental and theoretical advances. In this paper, we report the structural and physical properties of a new quaternary Ce-based heavy fermion compound, $Ce_2NiAl_6Si_5$, which was synthesized via the self-flux method. This compound forms a layered tetragonal structure (space group $P4/nmm$) with square nets of Ce atoms separated by Si-Al or Ni-Si-Ge layers. Specific heat measurements show a low-temperature Sommerfeld coefficient of 1.4 J/mol-Ce·K^2 with reduced entropy, indicative of significant Kondo interactions. Below 0.6 K, an increase in resistivity and a deviation in magnetic susceptibility suggest the appearance of magnetic ordering or the development of dynamic magnetic correlations, which is further supported by a bulge in the specific heat around 0.4 K. The findings of this study suggest that $Ce_2NiAl_6Si_5$ is a layered heavy fermion metal naturally located near a spin-density-wave quantum critical point.

DOI: 10.1088/0256-307X/41/12/127304

Introduction. Strong electronic correlations lead to enhanced electron effective masses and narrowed electronic bandwidths, as exemplified in heavy fermion metals, which can have electrons (fermions) with an effective mass over 1000 times the free electron mass, resulting from the hybridization between localized f-electrons and light conduction electrons.[1] The relatively small energy scales in heavy fermion metals allow for effective tuning of their ground states via non-thermal parameters, such as pressure, magnetic field, chemical doping, and dimensionality.[2–5] Magnetically ordered phases can be continuously suppressed using these non-thermal parameters, leading to quantum critical points (QCPs),[2] around which unconventional superconductivity and non-Fermi-liquid (NFL) behaviors have been observed.[6] Such QCPs have been extensively studied in anti-ferromagnetic (AFM) heavy fermion metals, such as $CeRhIn_5$,[7–9] $CePd_2Si_2$,[10] and $CeCu_{6-x}Au_x$[11]), and recently in ferromagnetic (FM) $CeRh_6Ge_4$.[12–14] The high tunability and abundance of ordered phases in heavy fermion metals make them ideal for studying quantum phase transitions and unconventional states of matter that emerge around QCPs[2,6,15–18], and motivate the search for new materials that are close to QCPs. Compounds with quasi-two-dimensional (2D) square lattices are particularly interesting because they may host physics similar to those of high-T_c superconducting cuprates[19,20] and iron pnictides/chalcogenides.[21–23]

Recently, the $Ce_2MAl_7Ge_4$ (M = Co, Ir, Ni, Pd) compound family was found to exhibit interesting physical properties.[24] These compounds crystallize in a non-centrosymmetric tetragonal structure (space group $P\bar{4}2_1m$) with quasi-2D Ce layers separated by Ge-Al and M-Al-Ge blocks.[24] $Ce_2PdAl_7Ge_4$ has been suggested to be at a QCP with NFL behavior extending down to 0.4 K, whereas other variants with M = Co, Ir, and Ni magnetically order at 1.8, 1.6, and 0.8 K, respectively.[24] In this study, we successfully synthesized a new heavy fermion metal, $Ce_2NiAl_6Si_5$, discovered while exploring the chemical pressure effects in $Ce_2NiAl_7Ge_4$, by partially replacing Ge with Si. Unlike $Ce_2MAl_7Ge_4$ compounds, $Ce_2NiAl_6Si_5$ crystallizes in a centrosymmetric tetragonal structure (space group $P4/nmm$). At approximately 0.6 K, an upturn in resistivity and a deviation from the Curie–Weiss behavior in magnetic susceptibility suggest the onset of AFM order or dynamic AFM correlations, which is also corroborated by a bulge in specific heat that occurs at a slightly lower temperature. A large Sommerfeld coefficient of 1.4 J/mol-Ce·K^2 at 0.1 K and a reduction in entropy indicate significant Kondo interactions in $Ce_2NiAl_6Si_5$. These findings indicate that $Ce_2NiAl_6Si_5$ is a square-lattice heavy fermion metal located close to a QCP and motivate further pressure- or field-tuning studies that directly access the QCP.

Experimental Methods. $Ce_2NiAl_6Si_5$ single crystals were synthesized using the Al/Si self-flux method. Ce rods (Alfa Aesar, 99.9%), Ni powder (PrMat 99.99%), Si ingots (PrMat 99.9999%), and Al granules (PrMat 99.9999%)

*Corresponding author. Email: liuyu002@mail.ustc.edu.cn; yusong_phys@zju.edu.cn; hqyuan@zju.edu.cn
© 2024 Chinese Physical Society and IOP Publishing Ltd

were placed in an alumina crucible with a molar ratio of Ce : Ni : Al : Si = 1 : 1 : 35 : 8 and sealed in an evacuated quartz ampoule. The ampoule was heated to 1100 ℃, held at this temperature for 24 h, and subsequently cooled slowly to 700 ℃. Finally, shiny platelet $Ce_2NiAl_6Si_5$ single crystals were obtained after centrifugation to remove the excess flux.

The chemical composition was determined via energy-dispersive spectroscopy (EDS) with a Hitachi SU8010 scanning electron microscope, which provided an atomic ratio of Ce : Ni : Al : Si = 14.82 : 7.55 : 40.29 : 37.34 (2 : 1.02 : 5.44 : 5.04). The crystal structure was characterized via single-crystal X-ray diffraction (XRD) using a Bruker D8 Venture diffractometer with Mo K_α radiation at room temperature. The electrical resistivity and heat capacity were measured using a Quantum Design physical property measurement system (PPMS) equipped with a dilution refrigerator. Magnetization measurements were performed using a Quantum Design magnetic property measurement system (MPMS) equipped with a ^{3}He refrigerator.

Results and Discussion. Refinement of the single crystal XRD results indicates that $Ce_2NiAl_6Si_5$ crystallizes in a defect variant of the Sm_2NiGa_{12} structure[25–27] with the centrosymmetric space group $P4/nmm$ (No. 129). Although the non-centrosymmetric space group $P\bar{4}2_1m$ yields better refinement in the $Ce_2MAl_7Ge_4$ family,[24] the higher-symmetry $P4/nmm$ space group yields better refinement than the $P\bar{4}2_1m$ space group ($wR_2 = 0.0736$) for $Ce_2NiAl_6Si_5$.

The refined crystal structures of $Ce_2NiAl_6Si_5$ are listed in Table 1. In this crystal structure, there are Ce and Ni sites at the $4f$ and $2b$ Wyckoff positions, respectively. There are two crystallographically inequivalent Al sites and three inequivalent Si sites. Similar to typical intermetallic compounds containing Al and Si, it is difficult to distinguish between these two elements using X-ray scattering.[28] We found that the model in Table 1 yields the lowest R-value in the refinement, although a similar R-value ($wR_2 = 0.0401$) is possible if Al(3) is assigned as Si; however, this is ruled out because it leads to a chemical composition inconsistent with the EDS measurements. Although our XRD measurements favor the crystal structure presented in Table 1, further neutron diffraction measurements are required to better distinguish between Al and Si.

Table 1. Crystal structure of $Ce_2NiAl_6Si_5$ determined from single-crystal XRD measurements at 300 K with Mo K_α radiation (0.71073 Å): $a = 5.86260(10)$ Å; $c = 14.7892(5)$ Å; $V = 508.31(2)$ Å^3; space group $P4/nmm$ (No. 129). Goodness of fit is 1.299, $R_1 = 0.0209$, $wR_2 = 0.0403$ (all data). The refined structural and isotropic displacement parameters U_{eq} are also shown, where U_{eq} is taken as 1/3 of the trace of the orthogonalized U_{ij} tensor.

Atoms	Wyck.	x	y	z	Occ.	U_{eq}(Å^2)
Ce(1)	$4f$	0.2500	0.7500	0.2357(1)	1	0.0075(2)
Ni(1)	$2b$	0.7500	0.2500	0.5000	1	0.0071(2)
Al(1)	$8j$	0.4958(1)	0.4958(1)	0.4118(1)	1	0.0081(2)
Al(2)	$2c$	0.7500	0.7500	0.1361(1)	1	0.0091(4)
Al(3)	$2c$	0.2500	0.2500	0.2974(1)	1	0.0043(4)
Si(1)	$2c$	0.7500	0.7500	0.3057(1)	1	0.0080(4)
Si(2)	$8j$	0.4572(1)	0.4572(1)	0.0771(1)	1	0.0140(2)

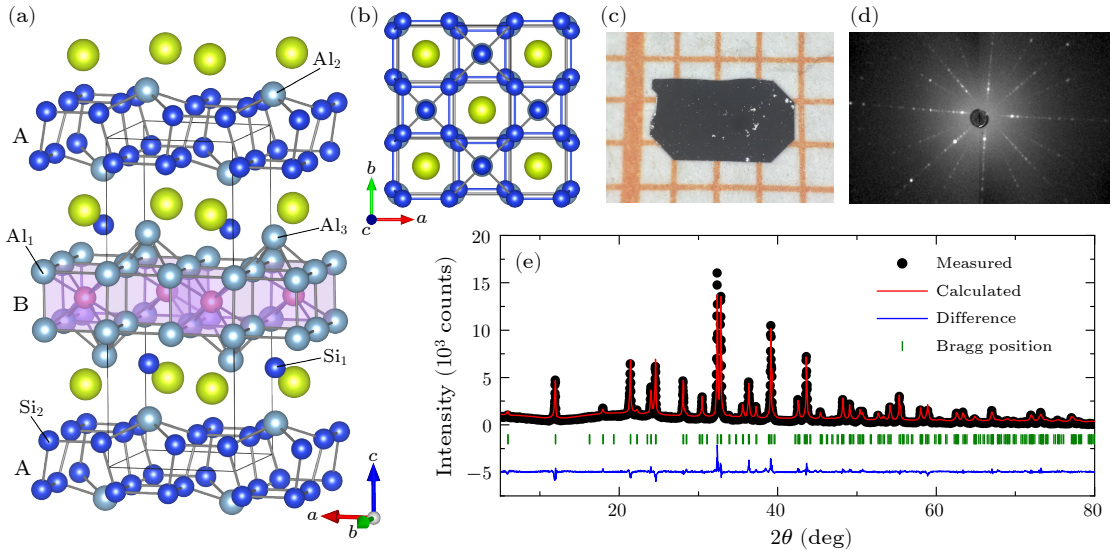

Fig. 1. (a), (b) $Ce_2NiAl_6Si_5$ crystal structure. The green, orange, gray, and blue spheres represent Ce, Ni, Al, and Si atoms, respectively. (c) Image of a $Ce_2NiAl_5Si_6$ crystal on a 1 × 1 mm grid. (d) Laue pattern of $Ce_2NiAl_6Si_5$. (e) Powder XRD data of $Ce_2NiAl_6Si_5$ at room temperature, with the corresponding Rietveld refinement shown as a solid line.

The $Ce_2NiAl_6Si_5$ crystal structure is shown in Figs. 1(a) and 1(b), with planar square nets of Ce atoms separated by alternating Al-Si (A-type) and Ni-Al-Si (B-type) layers along the c-axis. The intra-layer distance between Ce atoms is 4.15 Å, whereas the inter-layer distances between Ce atoms are 6.97 Å (separated by the A-type layer) and 7.82 Å (separated by the B-type layer), suggesting $Ce_2NiAl_6Si_5$ is a quasi-2D square lattice compound. The A-type layer is formed by Al(2) and Si(2) atoms, similar to the Al-Si layer in $Sm_2Ni(Ni_xSi_{1-x})Al_4Si_6$.[28] Compared with the A-type layer (formed by Al and Ge) in $Ce_2NiAl_7Ge_4$, which leads to a non-centrosymmetric structure, the A-type layer in $Ce_2NiAl_6Si_5$ has a different Al-Si pattern, resulting in an overall centrosymmetric structure. The B-type layer consists of five atomic layers stacked in an Al/Si-Al-Ni-Al-Al/Si sequence. The Ni atoms are surrounded by Al atoms, forming $NiAl_8$ distorted cubes. These $NiAl_8$ cubes are similar to the $NiGa_8$ cubes in Sm_2NiGa_{12},[25] the $NiAl_8$ cubes in $Ce_2NiAl_7Ge_4$,[24] and the $PtAl_8$ cubes in $CePtAl_4Si_2$.[29] Above and below the $NiAl_8$ cubes are Al(3) and Si(1) atoms, which have very close z-coordinates. Overall, the $Ce_2NiAl_6Si_5$ crystal structure is similar to that of $Ce_2NiAl_7Ge_4$, with the main difference being that the Al(3) and Si(1) sites in $Ce_2NiAl_6Si_5$ are occupied by Ge atoms in $Ce_2NiAl_7Ge_4$, which also changes the elemental atomic ratio from 2 : 1 : 6 : 5 to 2 : 1 : 7 : 4.

The $Ce_2NiAl_6Si_5$ crystal structure obtained via single-crystal XRD fully accounts for its powder XRD pattern, as shown in Fig. 1(e), and further confirms that the synthesized samples are single-phase with minimal excess flux. It is worth noting that while Al(3) and Si(1) are ordered in our refined structure, we cannot rule out mixing between the two sites because of the similarity between Al and Si, as observed via XRD. It is also possible that there may be Al deficiencies in our sample because energy-dispersive spectroscopy measurements suggest a value of ~ 5.4, which deviates from the ideal value of 6.

Figure 2(a) shows the temperature dependence of the $Ce_2NiAl_6Si_5$ electrical resistivity ρ_{ab}, with a broad hump at approximately 100 K. At low temperatures, ρ_{ab} drops sharply below 5 K and exhibits an upturn at approximately 0.6 K, as shown in the upper inset of Fig. 2(a). This upturn in $\rho(T)$ suggests the opening of an electronic gap, as observed in A-type $CeCu_2Si_2$,[30] YbBiPt,[31] and $CeRu_2Si_2$,[32] which may be due to spin-density-wave magnetic ordering in $Ce_2NiAl_6Si_5$ below 0.6 K. As shown in the lower inset of Fig. 2(a), the inter-layer resistivity ρ_c is significantly larger than ρ_{ab}. Upon cooling, ρ_c first increases and then decreases below 11 K, in contrast to ρ_{ab}. The strong anisotropy between ρ_{ab} and ρ_c is a characteristic of quasi-2D systems and is consistent with the layered structure of $Ce_2NiAl_6Si_5$.

The temperature dependence of the specific heat $C(T)/T$ of $Ce_2NiAl_6Si_5$ is shown in Fig. 2(b). In the paramagnetic state between 15 and 30 K, $C(T)/T$ was fitted using $C(T)/T = \gamma + \beta T^2$, yielding a Sommerfeld coefficient of $\gamma = 149.5(5)$ mJ/mol-Ce·K^2 and $\beta = 0.532(2)$ mJ/mol-Ce·K^4. A Debye temperature of $\Theta_D = 366.7$ K was calculated using $\Theta_D = \sqrt[3]{12\pi^4 nR/5\beta}$, where $n \approx 13.4$ is the number of atoms per formula unit and $R = 8.314$ J/mol·K. Below 12 K, $C(T)/T$ increases with decreasing temperature, and the electronic contribution to the specific heat $C_{el}(T)/T$ was estimated by subtracting the fitted phonon contribution. As shown in the inset in Fig. 2(b), a significant change in the $C_{el}(T)/T$ curve slope occurs at approximately 0.4 K. Although $C_{el}(T)/T$ does not decrease upon further cooling below 0.4 K, as expected in magnetically well-ordered metals, such a change in slope is consistent with magnetic ordering or the growth of magnetic correlations in heavy fermion systems near QCPs, with similar features seen in YbBiPt,[31] $CeCu_{1-x}Au_x$,[33] and $CeRh_6Ge_{4-x}Si_x$.[34] At the lowest measured temperature, $C_{el}(T)/T$ reaches a large γ value (1.4 J/mol-Ce·K^2) because of contributions from heavy electrons. The electronic entropy S_{el} was obtained by integrating $C_{el}(T)/T$ with respect to T, as shown in the inset of Fig. 2(b). The electronic entropy of $Ce_2NiAl_6Si_5$ per Ce is only 0.65 of $R\ln 2$ at 10 K, and recovers to $R\ln 2$ at approximately 20 K (not shown). This implies significant Kondo screening of Ce moments or magnetic correlations between Ce moments below 10 K.

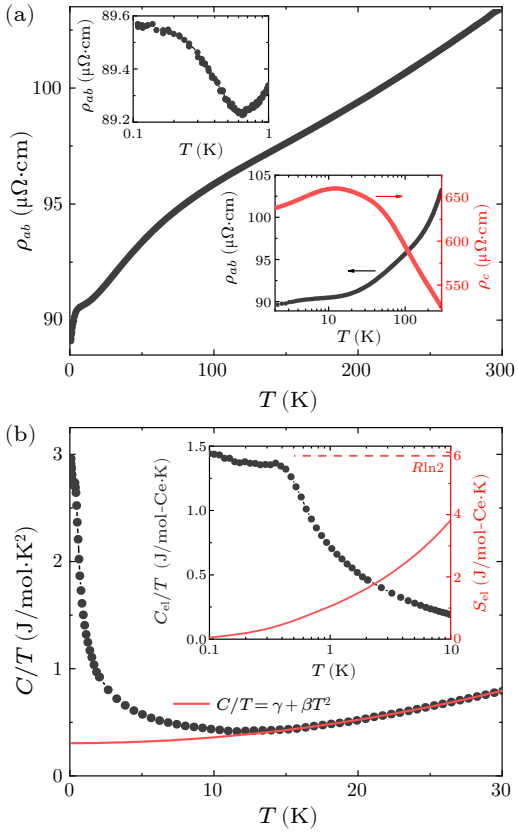

Fig. 2. (a) Temperature dependence of the resistivity $\rho_{ab}(T)$ of $Ce_2NiAl_6Si_5$. The upper inset zooms into ρ_{ab} below 1 K. The lower inset compares ρ_{ab} (left axis) and ρ_c (right axis). (b) Temperature dependence of the specific heat $C(T)/T$ of $Ce_2NiAl_6Si_5$. The inset shows the electron specific heat $C_{el}(T)/T$ (left axis) and entropy S_{el} (right axis).

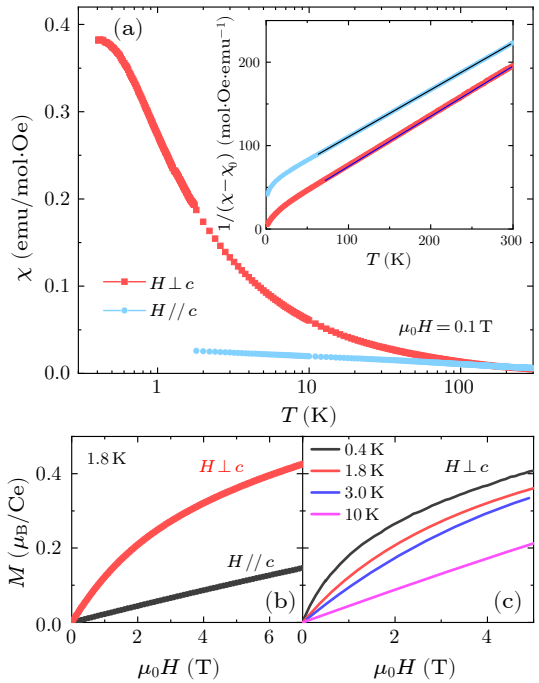

Fig. 3. (a) Temperature dependence of the magnetic susceptibility $\chi(T)$ at 0.1 T for $H \parallel c$ and $H \perp c$. The inset shows the inverse magnetic susceptibility $1/(\chi-\chi_0)$ for the two field directions. The solid lines are Curie-Weiss fits. (b) Field dependence of the magnetization of $Ce_2NiAl_6Si_5$ at 1.8 K for $H \parallel c$ and $H \perp c$. (c) Isothermal magnetization of $Ce_2NiAl_6Si_5$ at various temperatures for $H \perp c$.

Figure 3(a) shows the temperature dependence of the magnetic susceptibilities of $Ce_2NiAl_6Si_5$, measured at $\mu_0 H = 0.1$ T for $H \parallel c$ and $H \perp c$ [$\chi_\parallel(T)$ and $\chi_\perp(T)$]. Below 200 K, $\chi_\perp(T)$ is larger than $\chi_\parallel(T)$, indicating easy-plane magnetic anisotropy. As shown in the inset in Fig. 3(a), both $\chi_\parallel(T)$ and $\chi_\perp(T)$ of $Ce_2NiAl_6Si_5$ follow the Curie–Weiss law (for temperatures above ∼75 K), $\chi(\mathrm{T}) = \chi_0 + C/(T - \vartheta_\mathrm{p})$, where χ_0 is a temperature-independent term, $C = N_\mathrm{A}\mu_\mathrm{eff}^2/3k_\mathrm{B}$ is the Curie constant, and ϑ_p is the Weiss temperature. By fitting the $1/[\chi(T)-\chi_0]$ curves above 75 K to the Curie–Weiss model, an effective magnetic moment of $\mu_\mathrm{eff} = 2.69\mu_\mathrm{B}$/Ce, $\vartheta_\mathrm{p} = -95.6$ K, and $\chi_0 = 0.0016$ emu/mol·Oe were obtained for $H \parallel c$, while $\mu_\mathrm{eff} = 2.61\,\mu_\mathrm{B}$/Ce, $\vartheta_\mathrm{p} = -27.4$ K, and $\chi_0 = -0.0004$ emu/mol·Oe were obtained for $H \perp c$. These effective moment values yield a polycrystalline average of 2.64 μ_B/Ce for $Ce_2NiAl_6Si_5$, which is close to the 2.54 μ_B/Ce expected for Ce^{3+} free ions. For $H \perp c$, $\chi(T)$ of $Ce_2NiAl_6Si_5$ bends downward at approximately 0.6 K, suggesting the onset of the AFM order or the growth of dynamic AFM correlations.

The isothermal magnetization $M(H)$ of $Ce_2NiAl_6Si_5$ at 1.8 K is shown in Fig. 3(b). $M(H)$ is linear up to 7 T for $H \parallel c$, whereas for $H \perp c$ it is linear up to 1 T and then bends at higher fields without saturation up to 7 T. The polarized magnetic moment per Ce at 7 T is 0.44 μ_B for $H \perp c$, which is significantly smaller than the free Ce^{3+} ion moment. This may result from crystalline-electric field (CEF) effects, Kondo screening, or significant AFM interactions between the Ce moments. The $M(H)$ values of $Ce_2NiAl_6Si_5$ for $H \perp c$ at various temperatures are shown in Fig. 3(c). With increasing temperature, $M(H)$ for $H \perp c$ decreases in magnitude and the bending weakens.

Table 2. Energy levels and wave functions of the CEF scheme of $Ce_2NiAl_6Si_5$.

E (meV)	$\lvert -5/2\rangle$	$\lvert -3/2\rangle$	$\lvert -1/2\rangle$	$\lvert +1/2\rangle$	$\lvert +3/2\rangle$	$\lvert +5/2\rangle$
0	−0.426	0.0	0.877	0	−0.222	0.0
0	0.0	0.222	0.0	−0.877	0.0	0.426
2.42	−0.467	0.0	−0.003	0.0	0.884	0.0
2.42	0.0	0.884	0.0	−0.003	0.0	−0.467
9.73	0.775	0.0	0.481	0.0	0.411	0.0
9.73	0.0	0.411	0.0	0.481	0.0	0.775

By considering the local point-group symmetry of Ce ions, the anisotropic magnetic susceptibilities and isothermal magnetization can be modeled using an orthorhombic CEF Hamiltonian:

$$H_\mathrm{CEF} = B_2^0 O_2^0 + B_2^2 O_2^2 + B_4^0 O_2^4 + B_4^2 O_4^2 + B_4^4 O_4^4, \quad (1)$$

where B_i^n are the CEF parameters and O_i^n are the Stevens operators.[35] H_CEF leads to temperature-dependent magnetic susceptibility χ_CEF of isolated Ce^{3+} ions, and the inclusion of interactions between ions results in effective susceptibility $\chi_\mathrm{eff} = \chi_\mathrm{CEF}/(1 - \lambda\chi_\mathrm{CEF}) + \chi_0$, where χ_0 is a temperature-independent term and λ parameterizes the effective mean-field interaction. The magnetic susceptibility incorporating the CEF Hamiltonian was calculated using MantidPlot[36] and fitted to the data by minimizing $X^2 = (\chi_\mathrm{calc.} - \chi_\mathrm{obs.})^2/\chi_\mathrm{calc.}$, allowing for anisotropic values of λ and χ_0, yielding $X^2 = 0.189$ for the optimal fit. The extracted parameters are $B_2^0 = 0.23$ meV, $B_2^2 = 0.69938$ meV, $B_4^0 = 0.00031$ meV, $B_4^2 = 0.04972$ meV, $B_4^4 = 0.07812$ meV, $\lambda_\perp = -1.17$ mol/emu, $\lambda_\parallel = -76.29$ mol/emu, $\chi_0^\perp = -0.00008$ emu/mol, and $\chi_0^\parallel = 0.00091$ emu/mol. The energy levels and wave functions are summarized in Table 2, and the corresponding fitted susceptibilities are shown in Fig. 4. The CEF analysis results show that the $Ce_2NiAl_6Si_5$ ground state is a doublet with excited states at ∼2.4 and ∼9.7 meV. Further inelastic neutron scattering measurements are required to confirm the CEF scheme of $Ce_2NiAl_6Si_5$.

To confirm that the low-temperature anomalies in resistivity, magnetic susceptibility, and specific heat are associated with AFM ordering, the field-tuning of ρ_{ab} and $C(T)/T$ are shown in Fig. 5. The ρ_{ab} values of $Ce_2NiAl_6Si_5$ for fields along the c-axis and in the ab-plane are shown in Figs. 5(a) and 5(b), respectively. Although the resistivity upturn is suppressed towards lower temperatures in both cases, the response is highly anisotropic, with much faster

suppression for *ab*-plane fields, which is consistent with $Ce_2NiAl_6Si_5$ having an easy-plane magnetic anisotropy. Similarly, the bulge in the heat capacity is suppressed towards lower temperatures under an applied field, as shown in Fig. 5, which is consistent with the anomaly resulting from AFM ordering.

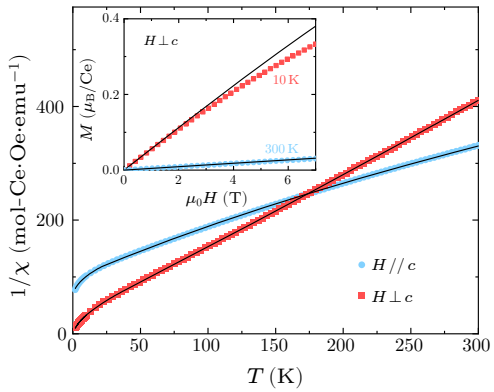

Fig. 4. $1/\chi(T)$ and $M(H)$ (inset) of $Ce_2NiAl_6Si_5$ fit to a CEF model (solid lines).

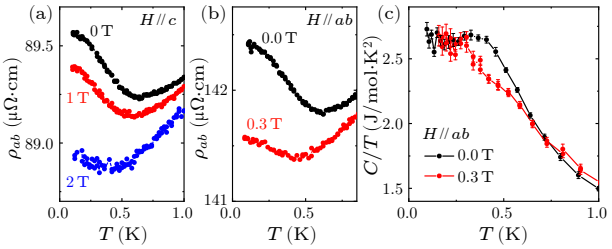

Fig. 5. ρ_{ab} of $Ce_2NiAl_6Si_5$ for fields (a) along the *c*-axis and (b) in the *ab*-plane. (c) $C(T)/T$ of $Ce_2NiAl_6Si_5$ for fields in the *ab*-plane.

Taken together, these $Ce_2NiAl_6Si_5$ characterizations are consistent with a heavy fermion metal that orders below 0.6 K, although the AFM ordering signatures are more subtle than those of well-ordered heavy fermion systems.[31] Compared with $Ce_2NiAl_6Si_5$, clearer magnetic ordering signatures were observed for $Ce_2NiAl_7Ge_4$ in specific heat at 0.8 K. This suggests that $Ce_2NiAl_7Ge_4$ has a more robust magnetic order than $Ce_2NiAl_6Si_5$, although the magnetic Bragg peaks are still too weak to be detected using neutron powder diffraction measurements.[24] Therefore, both $Ce_2NiAl_6Si_5$ and $Ce_2NiAl_7Ge_4$ are likely to be in proximity to QCPs, with $Ce_2NiAl_6Si_5$ having a weaker magnetic order and being closer to its QCP. Further neutron single-crystal diffraction measurements are required to elucidate the magnetic properties of $Ce_2NiAl_6Si_5$.

In summary, we successfully grew $Ce_2NiAl_6Si_5$ single crystals using the self-flux method, which crystallizes in a centrosymmetric tetragonal structure with space group $P4/nmm$ (No. 129). Electrical resistivity and magnetic susceptibility measurements suggest the onset of AFM ordering or dynamic AFM correlations at approximately 0.6 K, although the corresponding anomaly in specific heat appears at a slightly lower temperature (0.4 K). The large low-temperature $C(T)/T$ and reduced entropy indicate a significant Kondo effect. These results indicate that $Ce_2NiAl_6Si_5$ is a quasi-2D layered heavy fermion metal close to quantum criticality and motivate further systematic studies on its tunability under pressure or magnetic fields.

Acknowledgements. The work at Zhejiang University was supported by the Pioneer and Leading Goose R&D Program of Zhejiang Province, China (Grant No. 2022SDXHDX0005), the National Key R&D Program of China (Grant Nos. 2022YFA1402200 and 2023YFA1406100), the Key R&D Program of Zhejiang Province, China (Grant No. 2021C01002), the National Natural Science Foundation of China (Grant Nos. 12034017, 12274363, and 12350710785), and the Fundamental Research Funds for the Central Universities (Grant No. 226-2024-00068).

References

[1] Stewart G R 1984 *Rev. Mod. Phys.* **56** 755
[2] Weng Z F, Smidman M, Jiao L, Lu X, and Yuan H Q 2016 *Rep. Prog. Phys.* **79** 094503
[3] Chen Y, Weng Z F, Michael S, Lu X, and Yuan H Q 2016 *Chin. Phys. B* **25** 077401
[4] Smidman M, Shen B, Guo C Y, Jiao L, Lu X, and Yuan H Q 2019 *Chin. Phys. B* **28** 017106
[5] Xia X B, Shen B, Smidman M, Chen Y, Lee H, and Yuan H Q 2018 *Chin. Phys. Lett.* **35** 067102
[6] White B D, Thompson J D, and Maple M B 2015 *Physica C* **514** 246
[7] Park T, Ronning F, Yuan H Q, Salamon M B, Movshovich R, Sarrao J L, and Thompson J D 2006 *Nature* **440** 65
[8] Knebel G, Aoki D, Braithwaite D, Salce B, and Flouquet J 2006 *Phys. Rev. B* **74** 020501
[9] Jiao L, Chen Y, Kohama Y, Graf D, Bauer E D, Singleton J, Zhu J X, Weng Z F, Pang G M, Shang T, Zhang J L, Lee H O, Park T, Jaime M, Thompson J D, Steglich F, Si Q M, and Yuan H Q 2015 *Proc. Natl. Acad. Sci.* **112** 673
[10] Mathur N D, Grosche F M, Julian S R, Walker I R, Freye D M, Haselwimmer R K W, and Lonzarich G G 1998 *Nature* **394** 39
[11] Stockert O and Steglich F 2011 *Annu. Rev. Condens. Matter Phys.* **2** 79
[12] Matsuoka E, Hondo C, Fujii T, Oshima A, Sugawara H, Sakurai T, Ohta H, Kneidinger F, Salamakha L, Michor H, and Bauer E 2015 *J. Phys. Soc. Jpn.* **84** 073704
[13] Shen B, Zhang Y J, Komijani Y, Nicklas M, Borth R, Wang A, Chen Y, Nie Z Y, Li R, Lu X, Lee H O, Smidman M, Steglich F, Coleman P, and Yuan H Q 2020 *Nature* **579** 51
[14] Kotegawa H, Matsuoka E, Uga T, Takemura M, Manago M, Chikuchi N, Sugawara H, Tou H, and Harima H 2019 *J. Phys. Soc. Jpn.* **88** 093702
[15] Stewart G R 2001 *Rev. Mod. Phys.* **73** 797
[16] von Löhneysen H, Rosch A, Vojta M, and Wölfle P 2007 *Rev. Mod. Phys.* **79** 1015
[17] Pfleiderer C 2009 *Rev. Mod. Phys.* **81** 1551
[18] Si Q M and Steglich F 2010 *Science* **329** 1161
[19] Dagotto E 1994 *Rev. Mod. Phys.* **66** 763
[20] Leggett A J 2006 *Nat. Phys.* **2** 134
[21] Fernandes R M, Coldea A I, Ding H, Fisher I R, Hirschfeld P J, and Kotliar G 2022 *Nature* **601** 35
[22] Si Q M, Yu R, and Abrahams E 2016 *Nat. Rev. Mater.* **1** 16017
[23] Kang B L, Shi M Z, Zhao D, Li S J, Li J, Zheng L X, Song D W, Nie L P, Wu T, and Chen X H 2022 *Chin. Phys. Lett.* **39** 127401

[24] Ghimire N J, Cary S K, Eley S, Wakeham N A, Rosa P F S, Albrecht-Schmitt T, Lee Y, Janoschek M, Brown C M, Civale L, Thompson J D, Ronning F, and Bauer E D 2016 *Phys. Rev. B* **93** 205141
[25] Chen X Z, Small P, Sportouch S, Zhuravleva M, Brazis P, Kannewurf C R, and Kanatzidis M G 2000 *Chem. Mater.* **12** 2520
[26] Cho J Y, Millican J N, Capan C, Sokolov D A, Moldovan M, Karki A B, Young D P, Aronson M C, and Chan J Y 2008 *Chem. Mater.* **20** 6116
[27] Macaluso R T, Millican J N, Nakatsuji S, Lee H O, Carter B, Moreno N O, Fisk Z, and Chan J Y 2005 *J. Solid State Chem.* **178** 3547
[28] Chen X Z, Sportouch S, Sieve B, Brazis P, Kannewurf C R, Cowen J A, Patschke R, and Kanatzidis M G 1998 *Chem. Mater.* **10** 3202
[29] Ghimire N J, Ronning F, Williams D J, Scott B L, Luo Y K, Thompson J D, and Bauer E D 2014 *J. Phys.: Condens. Matter* **27** 025601
[30] Gegenwart P, Langhammer C, Geibel C, Helfrich R, Lang M, Sparn G, Steglich F, Horn R, Donnevert L, Link A, and Assmus W 1998 *Phys. Rev. Lett.* **81** 1501
[31] Fisk Z, Canfield P C, Beyermann W P, Thompson J D, Hundley M F, Ott H R, Felder E, Maple M B, Lopez de la Torre M A, Visani P, and Seaman C L 1991 *Phys. Rev. L* **67** 3310
[32] Miyako Y, Kawarazaki S, Taniguchi T, Takeuchi T, Marumoto K, Hamada R, Yamamoto Y, Sato M, Tabata Y, Tanabe H, Ocio M, Pari P, and Hammann J 1997 *Physica B: Condens. Matter* **230–232** 1011
[33] von Löhneysen H 1996 *J. Phys.: Condens. Matter* **8** 9689
[34] Zhang Y J, Nie Z Y, Li R, Li Y C, Yang D L, Shen B, Chen Y, Du F, Luo S S, Su H, Shi R, Wang S Y, Nicklas M, Steglich F, Smidman M, and Yuan H Q 2022 *Phys. Rev. B* **106** 054409
[35] Stevens K W H 1952 *Proc. Phys. Soc.* **65** 209
[36] Arnold O, Bilheux J C, Borreguero J M, Buts A, Campbell S I, Chapon L, Doucet M, Draper N, Ferraz Leal R, Gigg M A, Lynch V E, Markvardsen A, Mikkelson D J, Mikkelson R L, Miller R, Palmen K, Parker P, Passos G, Perring T G, Peterson P F, Ren S, Reuter M A, Savici A T, Taylor J W, Taylor R J, Tolchenov R, Zhou W, and Zikovsky J 2014 *Nucl. Instrum. Methods Phys. Res., Sect. A* **764** 156